

Fluid Model of an Electron Cyclotron Wave Resonance Discharge

Spyridon A. Sfikas, Eleftherios K. Amanatides, Dimitris S. Mataras, and Dimitrios E. Rapakoulas

Abstract—A fluid model of a planar electron cyclotron wave resonance Argon discharge is presented. The results for a 15-mtorr Argon discharge are checked against the particle in cell/Monte Carlo (PIC/MC) simulation results by R. Krimke *et al.* and are also compared to the analytical theory and experimental data by B. Pfeiffer. The application of a specific boundary condition for the magnetic potential, the use of an effective electron collision frequency that includes plasma nonuniformities, and the coupled solution of the electrostatic field were found to be essential parameters leading to the agreement of the fluid code with both experimental and PIC/MC findings.

Index Terms—Electron cyclotron wave resonance (ECWR), fluid model, inductively coupled plasma, RF discharges, self-consistent modeling.

I. INTRODUCTION

HIGH-DENSITY low-pressure plasmas, produced using electron cyclotron wave resonance (ECWR), have found applications in material processing. Under ECWR conditions, the inductively excited electron cyclotron waves propagate parallel to a weak—externally applied—static magnetic field, resulting in a resonance-like increase in plasma density [1], [2]. Fast self-consistent modeling of such a complex gas discharge is still a challenging task [3].

In this paper, we present a model of an ECWR Argon discharge in a 3-D infinite slab with symmetric y - z boundaries. The goal is to develop a fluid code capable of simulating reactive ECWR plasma processes. In this stage, the model was used for the simulation of low-pressure Argon discharges in resonant conditions. Specific boundary conditions (BCs) were implemented for the magnetic potential together with an effective electron collision frequency to account for plasma density inhomogeneities and to include the effects of the—externally applied—static magnetic field. Results concerning the distribution of plasma properties such as electron density, temperature, ion flux, and electrostatic field are presented and compared against previous experimental and modeling results [1], [2], [4].

II. MODEL DESCRIPTION

Fig. 1(a) shows the reactor geometry including the bounding dielectric walls and the direction of the static/alternative

magnetic field. The geometry is similar to those in [1], [2], and [4] and is actually a plasma slab of thickness $2d = 0.07$ m, bounded by two walls at $x = \pm d$. A static magnetic field $B_x = 2.25 \cdot 10^{-3}$ T is applied in the $+x$ -direction. Two conductive sheets carrying a 27.12-MHz frequency current, flowing in opposite ($\pm z$)-directions through a single-sector coils are positioned immediately outside the bounding walls. The simulated slab is part of a rectangular vacuum vessel filled with 15-mtorr Argon. For the particular value of the static magnetic field, the frequency of the alternative electromagnetic field is more than two times below electron cyclotron frequency. According to the experimental results of Pfeiffer [2], this value of the static magnetic field optimum power absorption can be achieved in the slab of specific dimensions and for a particular frequency value of the coil current. We shall call these particular conditions “resonant conditions”.

For the case presented here, the magnetic field is solved in the frequency domain while, for the electrostatic field and the charged species’ mass, momentum (for ions), and energy (for electrons) balance, we have employed a time step of $1.8436 \cdot 10^{-9}$ s. Finally, for neutral species, a time step of $1.8436 \cdot 10^{-7}$ s was used. The domain was split into 100 cells and the sheath structure was resolved by placing the grid points symmetrical to the y -axis, in distances decreasing gradually toward the walls (a geometric law using a value of 1.04 was applied). The particle, momentum, and energy balances were obtained from moments of the Boltzmann transport equation, coupled with Maxwell’s equations. The particle balance for electrons, ions, and neutrons is described by the continuity equation

$$\frac{\partial n_j}{\partial t} + \nabla \cdot \vec{\Gamma}_j = S \quad (1)$$

where n_j is the density, Γ_j is the flux of particle j , and S is the source of the particles consumed or produced in chemical reactions. In the present version, we have used a rather simplified chemistry of Ar discharges that includes two species (Ar and Ar^+) and three gas-phase reactions (ionization, momentum transfer, and electron-ion recombination). The rate constants for these reactions were calculated assuming a Maxwellian distribution while their cross sections were taken from [5].

The drift diffusion approximation replaces the momentum balance for the electrons

$$\vec{\Gamma}_e = -D_e \nabla n_e + \mu_e n_e \nabla \phi \quad (2)$$

Manuscript received February 15, 2007; revised July 4, 2007.

The authors are with the Plasma Technology Laboratory, Department of Chemical Engineering, University of Patras, 26504 Patras, Greece (e-mail: dim@plasmatech.gr).

Color versions of one or more of the figures in this paper are available online at <http://ieeexplore.ieee.org>.

Digital Object Identifier 10.1109/TPS.2007.905946

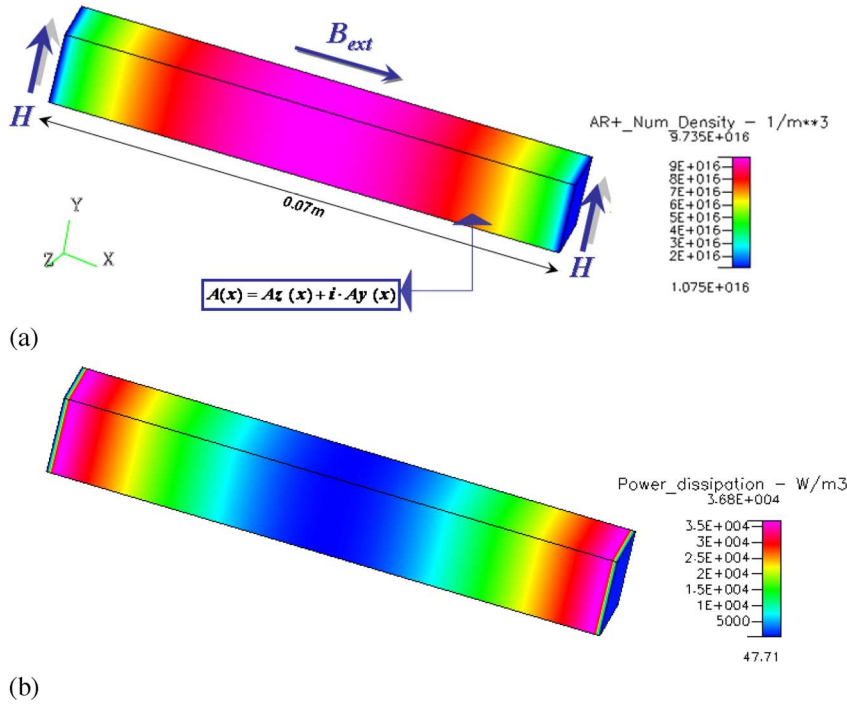


Fig. 1. (a) Geometrical model of the infinite in y - and z -directions' plasma slab, with the superimposed static magnetic field B_{ext} . The applied boundary condition for the vector magnetic potential and the ion density profile calculated by the simulation are also shown. (b) Spatial distribution of the simulated inductive power dissipation in the discharge.

where n_e is electron density, μ_e is the electron mobility, D_e is the diffusion coefficient, and ϕ is the electrostatic potential. The transport coefficients μ_e and D_e were derived from the two-term expansion of the Boltzmann equation

$$T_e \mu_e = D_e = \frac{2e}{3m_e n_e} \cdot \int_0^{\infty} \frac{\varepsilon^{3/2}}{\nu_{eff}(\varepsilon)} \cdot f(\varepsilon) d\varepsilon \quad (3)$$

where a Maxwellian electron energy distribution is assumed, and $\nu_{eff}(\varepsilon)$ is the effective collision frequency as defined in (4).

The definition of scalar instead of tensor diffusion and mobility coefficients is used since the model is essentially 1-D (the symmetric y - z boundaries are used only for the creation of the high-frequency (hf) electromagnetic field through the application of the specific BCs for the magnetic potential).

Furthermore, we have applied a modified effective collision frequency ν_{eff} [6] of the form

$$\nu_{eff} = \left[1 + \left(\frac{\omega_c \cdot \frac{N_e}{N_{eRES}}}{\nu} \right)^2 \right] \cdot \nu \quad (4)$$

where $\omega_c = 3.956 \cdot 10^8 \text{ s}^{-1}$ is the electron cyclotron frequency, ν is the collision frequency as in [7], N_e is the electron density, and N_{eRES} is the electron density in resonant conditions, i.e., $1 \cdot 10^{11} \text{ cm}^{-3}$ for the specific set of conditions. Equation (4) essentially represents the effect of electron motion in the y - and z -directions on the x -direction. In addition, it is used in order to describe a phenomena that cannot be illustrated by the drift-diffusion approximation as inertia and diamagnetic forces. Thus, (4) is used to reflect the fact that there is a parallel force

pushing the electrons against the gradients of the magnetic field and that their motion along it is not actually unhindered [8]. According to Pfeiffer's experiments, N_e was kept constant at a value of $1 \cdot 10^{11} \text{ cm}^{-3}$ while varying the static magnetic field B_0 and the rf coil voltage V_{rf} . The minimum in the $V_{rf} = f(B_0)$ curve is a characteristic feature, and the static magnetic field $B_0 = 2.25 \text{ mT}$ at the voltage minimum indicates the resonance. Pfeiffer's equations apply for a spatially homogeneous plasma [$N_e(x) = N_e$]. If we define $N_{eRES} = 1 \cdot 10^{11} \text{ cm}^{-3}$, the gradient term N_e/N_{eRES} indicates the slab density nonuniformity that has to be taken into account in calculating the effective collision frequency as a function of $\omega_c = eB_0/m_e$ in (4).

On the other hand, the momentum balance equation is solved for the ions

$$\frac{\partial n_i u_i}{\partial t} + \nabla \cdot n_i \cdot u_i \cdot u_i = \frac{1}{m_i} \nabla \cdot (k_B n_i T_i) + \frac{q_i e}{m_i} E_{st} \cdot n_i - \nu_{im} n_i u_i \quad (5)$$

in order to include ion inertial effect due to the low number of ion-molecule collisions. In (5), u_i is the ion drift velocity, T_i is the ion temperature that is set equal to the gas temperature, m_i is the ion mass, E_{st} is the electrostatic field vector, and ν_{im} is the ion-molecule collision frequency, which is calculated from the ionic mobility μ_i according to the relation $\nu_{im} = e/m_e \mu_i$. In turn, the low field ionic mobility is calculated from Einstein's relation.

The energy balance is solved only for electrons, assuming that ions have equal energy with neutrals. The electron

temperature T_e is derived from the electron energy balance

$$\begin{aligned} \frac{3}{2} \frac{\partial}{\partial t} (n_e T_e) + \nabla \cdot \left(\frac{5}{2} T_e \vec{\Gamma}_e - \frac{5}{2} n_e D_e \cdot \nabla T_e \right) \\ = P - n_e \sum_i N_i K_i \quad (6) \end{aligned}$$

where the energy transfer is due to convective flux and thermodiffusion, and P is the power absorbed by electrons and is further analyzed to joule heating and inductive heating. The last term on the right side of (6) is the rate of electron power losses due to electron impact collisions. The deceleration of electrons in the sheath due to sheath potential has not currently been taken into consideration.

The system of equations is complemented by a set of BCs concerning the species' densities, as well as the electrostatic and electromagnetic potentials.

For a very rapid estimation of the basic plasma parameters, a fixed value close to ionization potential or a zero electric potential—as in the presented simulation case—BC in (2) has been applied to the walls. This BC leads to a very fast convergence but also to an overestimation of the electrostatic potential, ion current, and ion velocity toward the walls. We have also simulated a geometrically extended (and more time-consuming) case that takes into account the bounding dielectric walls and the current sheets immediately after them, resulting to an improved—nevertheless not drastically different—estimation of the previous parameters.

For the vector of the hf (27.12 MHz) magnetic potential $A(x)$, we have used a boundary condition of the form

$$A(x) = A_z(x) + i \cdot A_y(x) \quad (7)$$

where the $e^{j\omega t}$ time dependence has been eliminated, and $A_z(x)$ and $A_y(x)$ account for the analysis of the total magnetic vector potential to an H_y and an $i \cdot H_z$ superposition. The values of $A_z(x)$ and $A_y(x)$ are given from the relations

$$\begin{aligned} A_z(x) = -C_1 \times \{ C_2 [\sin \gamma_2 x - \sin(-\gamma_2 x)] \\ + C_3 [\exp \gamma_1 x - \exp(-\gamma_1 x)] \} \quad (8) \end{aligned}$$

$$\begin{aligned} A_y(x) = C_1 \times \{ C_2 [\sin \gamma_2 x - \sin(-\gamma_2 x)] \\ - C_3 [\exp \gamma_1 x - \exp(-\gamma_1 x)] \} \quad (9) \end{aligned}$$

where γ_1 and γ_2 are the wavenumbers of the left-hand polarized (LHP) and right-hand polarized (RHP) waves, respectively. C_1 , C_2 , and C_3 result from the integration of equations (9a) and (9b) in [1] and can be expressed as

$$C_1 = \mu_0 \cdot H_s / 2 \quad (10)$$

$$C_2 = 1 / \{ \gamma_2 [\cos(\gamma_2 \cdot d) + \cos(-\gamma_2 \cdot d)] \} \quad (11)$$

$$C_3 = 1 / \{ \gamma_1 [\exp(\gamma_1 \cdot d) + \exp(-\gamma_1 \cdot d)] \} \quad (12)$$

where H_s is the hf magnetic field in the walls, μ_0 is the permeability of vacuum, and d is half of the slab length. The value of H_s for the results presented here is taken from the

experimental data in [2]. In addition, γ_1 and γ_2 are calculated as a function of the refractive index of the LHP and RHP wave n_l and n_r , respectively. For the calculation of the boundary condition for the magnetic potential, we have used a collision rate of $5 \cdot 10^7 \text{ s}^{-1}$. In addition, only the real (imaginary) part of the square of the refractive index n_r^2 (n_l^2) was taken into consideration. It is worth noticing that, for these specific conditions, the imaginary part of n_l^2 for the LHP wave is much larger than the real part, indicating a strong skin effect. The opposite is true for the RHP wave, where the real part of n_r^2 is much larger and determines its propagation. For the calculated values of n_r^2 and n_l^2 , assuming a collision frequency of $5 \cdot 10^7 \text{ s}^{-1}$, nearly half a wavelength of the RHP wave fits into the slab.

Moreover, the electron flux normal to the surfaces was set as

$$\vec{\Gamma}_{e,n} = \frac{1}{4} n_e \nu_{e,\text{th}}; \quad \nu_{e,\text{th}} = \left[\frac{8k_B T_e}{\pi m_e} \right]^{\frac{1}{2}} \quad (13)$$

where $\nu_{e,\text{th}}$ is the electron thermal velocity, k_B is the Boltzmann constant, and m_e is the electron mass.

As for the boundary condition for electron temperature (6), the thermal flux balance condition was assumed after taking into account the quite high values of the electrostatic field close to the surfaces. In such a manner, the electron temperature at the walls becomes

$$\frac{5}{2} \cdot T_e \cdot \Gamma_{e,n} - \frac{5}{2} \cdot n_e \cdot D_e \cdot \nabla T_e = 2 \cdot T_e \frac{1}{4} \cdot n_e \cdot u_{e,\text{th}} \quad (14)$$

assuming no secondary electron emission. The ion flux at the surfaces is calculated by taking into account the probability of ion-surface recombination resulting in a flux balance of the form

$$\vec{\Gamma}_{i,n} = s_i n_i u_{i,w} \quad (15)$$

where the value of s_i (sticking coefficient denoting the probability of electron-ion recombination) in (15) has been set to unity, and the drift velocity toward the walls $u_{i,w}$ is equalized with the ion drift velocity in a distance of one mean free path from the surface, which, in turn, is estimated from ion mobility and electrostatic field intensity.

III. RESULTS AND DISCUSSION

Fig. 1(a) and (b) shows the distribution of Argon ion density and inductive heating in the slab. Ion density is uniform in the y - and z -directions, while, in the x -direction, it is maximized in the middle of the slab and vanishes toward the conductive sheets ($x = \pm d$). The distribution of inductive heating, calculated as $P_{\text{ind}} = 1/2 \cdot \text{Re}(\sigma) \cdot E_{\text{RF}}^2$ where $\sigma = (\varepsilon_0 \cdot \omega_p) / (\nu_{\text{eff}} + i \cdot \omega)$ is the plasma conductivity and $E_{\text{RF}} = \sqrt{\omega^2 \cdot A_y^2 + \omega^2 \cdot A_z^2}$ is the modulus of the induced electric field, as in the case of ion density, is uniform in the y - and z -directions. In the x -direction instead, it presents two peaks close to the $x = \pm d$ and is about zero in the middle of the slab as the induced electric field is very small in this area. It is worth noticing that inductive heating is the main mechanism of energy absorption in these conditions,

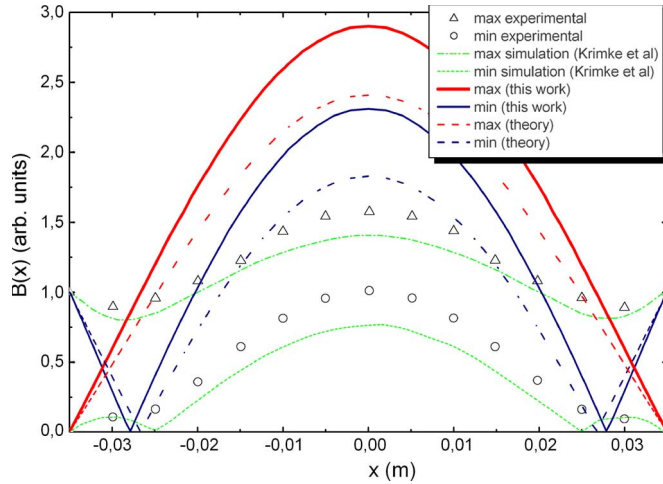


Fig. 2. Maximum and minimum hf magnetic field as calculated in the present simulation and compared to other simulation results [4] and experimental data [3]. Theoretical results [2] for a homogeneous density profile of $N_e = 1 \cdot 10^{11} \text{ cm}^{-3}$ and a zero collision rate are also shown.

whereas Joule heating calculated as $P_{\text{joule}} = e \cdot \vec{\Gamma}_e \cdot \nabla \phi$ can play a role only when very close to the dielectric walls.

In Fig. 2, we compare the results of our simulation for the maximum and minimum hf magnetic field, with B. Pfeiffer's simplified analytical theory [2] and experimental data [3] and the simulation results published by Krimke *et al.* [4]. The terms “maximum” and “minimum” hf magnetic field refer to the z - and y -components of the hf magnetic field $i \cdot H_z = i \cdot (H_R - H_L)$ and $H_y = H_R + H_L$, where H_R is the RHP and H_L the LHP contribution as in [2]. The boundary condition introduced for the vector magnetic potential (7) produces an hf magnetic field distribution that is close to the analytical theory for zero collision rate and deviates from the experimental and PIC/MC results only in the area close to the conductive sheets. In addition, the maximum hf magnetic field reached the value of $0.15 \cdot 10^{-4} \text{ T}$ at the walls ($x = \pm d$) as it should [3], but a deviation from the theory and experiment is observed mainly in the center of the discharge slab, a region with low induced electric field and power dissipation.

Despite the overestimation of the magnetic field in the middle of the slab, plasma properties are well predicted as shown in Fig. 3(a) and (b). Fig. 3(a) shows the distribution of electron density in the x -direction of the slab, and a fairly good agreement was found between the fluid simulation and PIC/MC results [4], which are also included in the figure together with Schottky theory prediction. The maximum value of N_e is $\sim 1 \cdot 10^{17} \text{ m}^{-3}$, which is equal to the value used in the analytical calculations of [1]. Furthermore, the model prediction of electron temperature T_e is shown in Fig. 3(b), and a slight overestimation of the results of fluid simulation compared to PIC/MC model was found. This overestimation is stronger near the conductive sheets and comes from the rather localized inductive heating [Fig. 2(b)] and the contribution of Joule heating in this area, which were described above.

Fig. 4(a) shows the plasma electrostatic potential Φ , which has a gradient profile and a maximum value of 14.85 V. Both the shape and the values of the electrostatic potential are identical to the results of [4], included in the figure. It is noticeable

that this agreement was possible only after the coupling of the Poisson's relation to the fluid code, i.e., the assumption of quasi-neutrality and ambipolarity led always to a strong underestimation of the electrostatic potential. Moreover, Fig. 4(b) shows the calculated profile of the maximum induced electric field E_{RF} . We compare the value of [4] for the maximum induced electric field with the value obtained assuming a uniform plasma density to demonstrate the effectiveness of the applied boundary condition for the magnetic potential under specific conditions. The induced field is maximized at the walls, where it has a maximum value of 166.5 V. This value is $\sim 30\%$ lower than the maximum value calculated by the PIC/MC simulation, and this deviation is directly related to the differences in the magnetic field distribution, which were shown in Fig. 2. The rather small changes between the maximum and minimum values of the magnetic field near the walls finally lead to a rather smooth change of the induced field close to the conductive walls.

Finally, Fig. 5 shows the ion drift velocity v_i in the x -direction of the slab as calculated from our simulation and the PIC/MC code. One can observe that, in the center of the slab, the differences are rather small (less than 5%) and increase when close to the walls. As a result, the maximum ion current density ($x = \pm d$) was found to be $J_i = 1.3 \text{ mA} \cdot \text{cm}^{-2}$ while, in [4], a saturation current of $0.77 \text{ mA} \cdot \text{cm}^{-2}$ was calculated. We believe that this divergence comes from our consideration of the wall as a conductive with a boundary condition for the electrostatic potential equal to zero. This, in turn, results in a much stronger electrostatic field near the walls and overestimates the ion drift velocity.

IV. CONCLUSION

A fluid code was developed for the simulation of ECWR 15-mTorr Argon discharges in an infinite slab. A modified boundary condition was used for the magnetic potential in order to include the effect of the weak—externally applied—static magnetic field on the plasma properties. Moreover, a modified effective electron collision frequency was implemented in order to include, in our model, plasma density nonuniformities. The results for the hf magnetic field are in reasonable agreement with experimental data, while, for plasma properties such as electron density, electron temperature, and electrostatic potential, good agreement was found with PIC/MC simulation results. Significant deviations between the fluid and the PIC/MC codes were found only for the ion flux density, and this difference is attributed to the electrostatic field calculations close to the walls. The model can be further enhanced with the introduction of a parametric boundary condition for the magnetic potential and an improved plasma conductivity calculation through the Appleton–Hartree tensor. The main purpose of the development of this code is to be later extended and applied to complicated gas phase and surface chemistries and plasma processes that use ECWR sources. From this point of view, the development of a fluid code that can reproduce experimental and Monte Carlo simulation results is very important because it will reduce the computational time and will allow for a higher dimensionality.

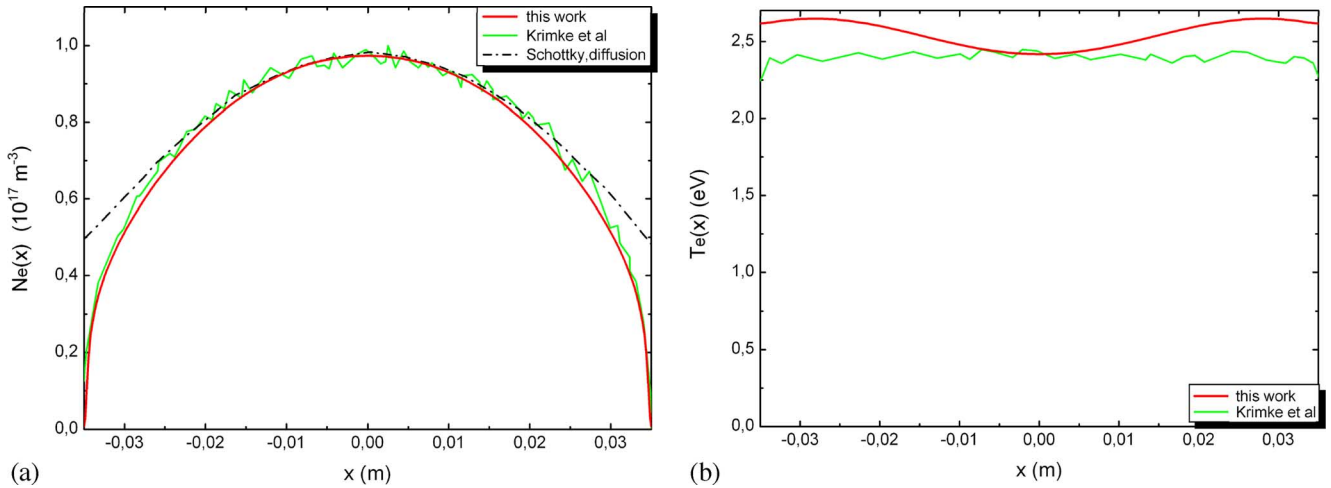


Fig. 3. (a) Plasma electron density N_e and (b) electron temperature T_e , as calculated in this simulation and compared to the simulation results of [4]. The Schottky diffusion profile is also indicated in (a).

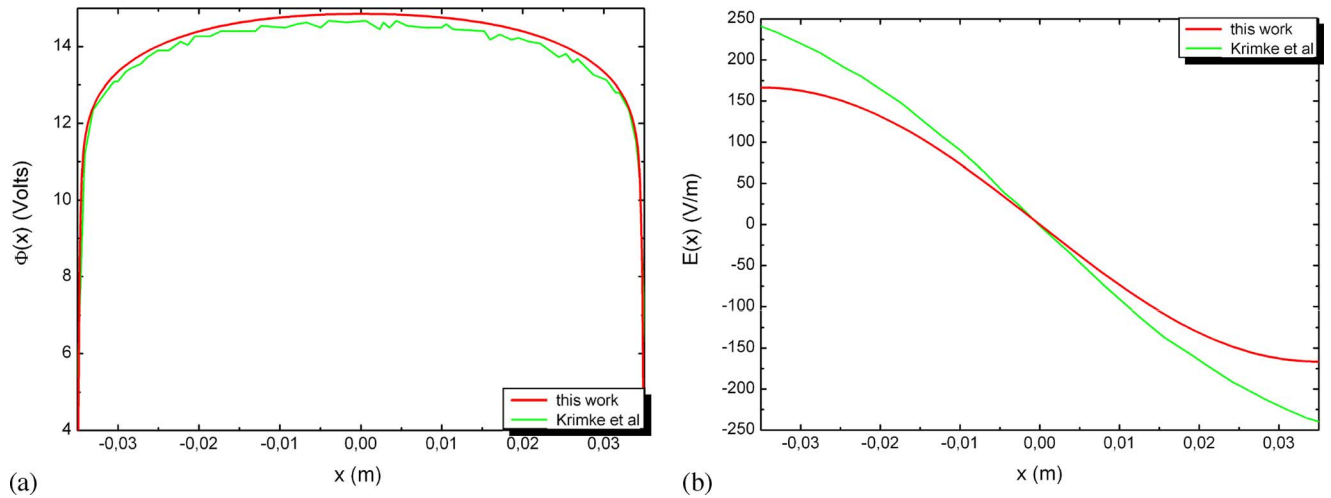


Fig. 4. (a) Potential Φ and (b) maximum induced electric field E , as calculated in this simulation and compared to the simulation results of [4].

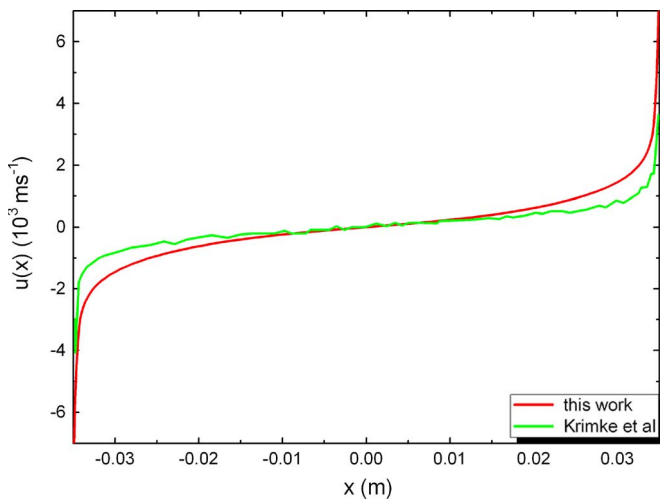


Fig. 5. Ion drift velocity u as calculated in this simulation and compared to the simulation results of [4].

REFERENCES

- [1] B. Pfeiffer, "Skin effect in anisotropic plasmas and resonance excitation of electron-cyclotron waves. I. Theory," *J. Appl. Phys.*, vol. 37, no. 4, pp. 1624–1627, Mar. 1966.
- [2] B. Pfeiffer, "Skin effect in anisotropic plasmas and resonance excitation of electron-cyclotron waves. II. Experiments," *J. Appl. Phys.*, vol. 37, no. 4, pp. 1628–1633, Mar. 1966.
- [3] O. V. Polomarov, C. E. Theodosiou, I. D. Kaganovich, D. J. Economou, and B. N. Ramamurthi, "Self-consistent modeling of nonlocal inductively coupled plasmas," *IEEE Trans. Plasma Sci.*, vol. 34, no. 3, pp. 767–785, Jun. 2006.
- [4] R. Krimke and H. M. Urbasek, "Self-consistent simulation of a planar electron-cyclotron wave resonance discharge," *J. Appl. Phys.*, vol. 81, no. 11, pp. 7163–7169, Jun. 1997.
- [5] *University of Colorado ftp With Argon Collision Cross Section Database*. [Online]. Available: ftp://jila.colorado.edu/collision_data/
- [6] R. Winkler, V. A. Maiorov, and F. Sigeneger, "Impact of magnetic fields on the spatial relaxation of electrons," *J. Appl. Phys.*, vol. 87, no. 6, pp. 2708–2718, Mar. 2000.
- [7] F. F. Chen, "Collisional, magnetic, and nonlinear skin effect in radio-frequency plasmas," *Phys. Plasmas*, vol. 8, no. 6, pp. 3008–3017, Jun. 2001.
- [8] G. J. M. Hagelaar, "Modelling electron transport in magnetized low-temperature discharge plasmas," *Plasma Sources Sci. Technol.*, vol. 16, no. 1, pp. S57–S66, Feb. 2007.



Spyridon A. Sfikas grew up in Nafpaktos, Greece. He received the degree in electrical engineering from Patras Polytechnic University, Patras, Greece, in 1994. He is currently working toward the Ph.D. degree in the Plasma Technology Laboratory, Department of Chemical Engineering, University of Patras, Patras, Greece.

He was a Teacher of Technology and Industrial Arts in many secondary education schools. His current research interest focuses on the development of a fluid code capable of simulating low-pressure magnetically enhanced plasmas.



Dimitris S. Mataras received the Ph.D. degree in chemical engineering from the Department of Chemical Engineering, University of Patras, Patras, Greece, in 1990.

He is currently an Associate Professor with the Department of Chemical Engineering, University of Patras. His research interests are in the areas of plasma-enhanced CVD of various thin films, particularly amorphous and microcrystalline silicon, plasma diagnostics, and modeling, as well as plasma–surface interaction.



Eleftherios K. Amanatides was born in Athens, Greece, in 1972. He received the B.S. degree in chemistry from the University of Ioannina, Ioannina, Greece, in 1995 and the Ph.D. degree in chemical engineering, specializing in optimization of plasma-enhanced chemical vapor deposition in variable frequency reactors, from the University of Patras, Patras, Greece, in 2001.

He is currently a Research Fellow with the Plasma Technology Laboratory, University of Patras, where he is primarily involved with the development of

dual frequency low-pressure plasma sources, the development of new plasma diagnostics, and the simulation of plasma-enhanced chemical vapor deposition of thin films used in solar cells and in biomedical applications.



Dimitrios E. Rapakoulias was born in Athens, Greece, in 1945. He received the B.S. degree in chemistry from the University of Athens, Athens, Greece, in 1971 and the Doctorat d'Etat in plasma chemistry from the Universite PARIS VI, Paris, France, in 1979.

From 1979 to 1982, he was a Maitre Assistant with the Department of Chemical Engineering, Universite PARIS VI. Since 1984, he has been with the Department of Chemical Engineering, University of Patras, Patras, Greece, where he is currently a

Professor in physical chemistry. During his career, he has developed expertise in the specialized areas of plasma chemistry including the fundamental aspects of gas-field and plasma–surface interactions, as well as applications in thin-film production for photovoltaic cells' (a-Si:H) diamondlike and polymerlike coatings. He had served in the past (1982–1985) as a General Secretary with the Ministry of Research and Technology, Greece, and as a General Manager with the Hellenic Institute of Pasteur (1988–1994). He has also been a chairman, cochairman, and member of scientific committees in several plasma processing and solar energy conferences.